NASA Technical Memorandum

NASA TM 82567

LOW LOSS INJECTOR FOR SPACE SHUTTLE MAIN ENGINE

Center Director's Discretionary Fund

Final Report

By George L. von Pragenau
Systems Dynamics Laboratory

February 1984

National Aeronautics and
Space Administration

George C. Marshall Space Flight Center

MSFC - Form 3190 (Rev. May 1983)

TECHNICAL REPORT STANDARD TITLE PAGE

1. REPORT NO.	2. GOVERNMENT ACCESSION NO.	3. RECIPIENT'S CATALOG NO.
NASA TM-82567		

4. TITLE AND SUBTITLE	5. REPORT DATE
Low Loss Injector for Space Shuttle Main Engine Center Director's Discretionary Fund, Final Report	February 1984 6. PERFORMING ORGANIZATION CODE
7. AUTHOR(S) George L. von Pragenau	8. PERFORMING ORGANIZATION REPORT #
9. PERFORMING ORGANIZATION NAME AND ADDRESS George C. Marshall Space Flight Center Marshall Space Flight Center, Alabama 35812	10. WORK UNIT, NO. 11. CONTRACT OR GRANT NO.
12. SPONSORING AGENCY NAME AND ADDRESS National Aeronautics and Space Administration Washington, D.C. 20546	13. TYPE OF REPORT & PERIOD COVERED Technical Memorandum 14. SPONSORING AGENCY CODE

15. SUPPLEMENTARY NOTES

Prepared by Systems Dynamics Laboratory, Science and Engineering Directorate

16. ABSTRACT

An efficient propellant injection method is discussed to raise the Space Shuttle Main Engine (SSME) thrust and payload. Relatively large diameter injector elements with low pressure loss are recommended for the main combustion chamber and the pre-burners. Smaller losses admit more propellant flow which then raises thrust. Payload is not only gained by specific impulse but also by thrust. The chamber pressure is stabilized by selecting the proper cavity size for the injector elements while reducing the injection pressure loss which normally is kept high for stability. The rather large injector element recesses provide acoustic damping which makes baffles and acoustic absorbers unnecessary. The study shows a tenfold reduction of flow induced stresses which are rather high in the present design. Relaxed tolerances, fewer elements, and better maintenance are offered. The study was conducted under a center director discretionary fund assignment.

17. KEY WORDS	18. DISTRIBUTION STATEMENT
Liquid propulsion engine Combustion devices Injectors Injector elements Injuector losses Combustion stability	Unclassified – Unlimited

19. SECURITY CLASSIF. (of this report)	20. SECURITY CLASSIF. (of this page)	21. NO. OF PAGES	22. PRICE
Unclassified	Unclassified	20	NTIS

For sale by National Technical Information Service, Springfield, Virginia 22151

TABLE OF CONTENTS

LIST OF ILLUSTRATIONS

TECHNICAL MEMORANDUM

LOW LOSS INJECTOR FOR SPACE SHUTTLE MAIN ENGINE

CURRENT INJECTOR DESIGN

Figure 1 shows a cut through the Space Shuttle Main Engine (SSME) power head assembly exhibiting forests of pencil-like injector elements. Figures 2, 3, and 4 are coaxial injector elements for the oxidizer (OPB) and fuel (FPB) preburners, and the main combustion chamber (MCC). The main injector assembly is seen in Figure 5 with one circular and five radial baffles extending from the primary face plate. The coaxial injector element feeds lox through a center tube (also lox post) from the lox dome into the combustion chamber. A cylindrical shroud around the lox post tip channels the fuel flow. The solid cylindrical lox jet is thus imbeded in a cylindrical coat of fuel upon discharging into the combustion chamber. The coaxial arrangement ensures good mixing and better stability than impinging jets. The fuel jet is by one magnitude faster than the lox jet for efficient mixing.

Each lox post is metered through an orifice at the post's inlet (Figs. 1 and 4). The fuel floods the lox post forest and enters through radial holes (Figs. 2 and 3) into the shrouds about the lox post tips. The radial holes meter the fuel flow. The preburner fuel is heated liquid hydrogen from the SSME nozzle cooling jacket while the MCC fuel is the hot turbine discharge gas from the high pressure oxidizer turbopump (HPOTP) and the high pressure fuel turbopump (HPFTP). The hot gas is fuel rich 0.84 part oxygen. Direct lox injection into the MCC raises the mixture ratio to 6 (oxygen/hydrogen) to produce a high specific impulse of 453 s in vacuum.

The hot gas rushes from the turbine discharges through lateral transfer ducts to the main injector (Fig. 1). The hot gas blast causes high bending stresses in the lox posts of the outer row which faces the transfer ducts from the HPFTP. The nonuniform flow distribution peaks at a velocity of 1200 ft/sec. Drag forces orthognally superimposed with the vortex lift forces contribute to high cycle fatigue. Four flat helix stringers are machined on the lox posts' surfaces as vortex spoilers. The flow shields of Figure 6 were added to bypass the hot gas loads in the outer row posts where the gas velocities are highest.

The injector elements have a high flow resistance to stabilize combustion. Propellant flow fluctuations are thus kept low even when the combustion pressure oscillates. The lox feed line ripple is attenuated with an accumulator (pogo suppressor) to uncouple low frequency (2 Hz) longitudinal vehicle resonances. Regenerative feedback between SSME thrust and lox feed system vibrations is thus avoided. Very high frequency combustion oscillations above 2000 Hz are damped by baffles and acoustic absorbers. The absorbers are tuned to the resonance of the partitions that are formed in the MCC by baffles. The absorber cavities are cooled with heated hydrogen, but combustion gases can enter to keep the cavities tuned to the MCC's temperature changes. The acoustic absorbers are imbedded in the upper corner of the MCC.

The OPB and FPB injector elements of Figure 2 are also coaxial. Their environment is less severe when compared to the MCC. Stability is provided through 3 radial baffles per chamber, conic corner liners, and a high injector pressure loss. The preburner lox flow is regulated by valves to control the SSME thrust and mixture ratio.

PROPOSED INJECTOR ELEMENT

Figure 7 gives the full scale cross section of the proposed MCC low loss injector element. All elements are arranged in the circularized hexagonal pattern of Figure 8 to minimize the exposed area of the primary faceplate. The lox posts are the structural backbone of each element. They are inertially welded, as in the present design, to the wall of the lox dome from where lox flows through individual holes into the lox posts. The holes are nonrestrictive, contrary to the orifices of the present design (Fig. 1).

The lox flow is metered by the sieve in the lox plug (Fig. 7). The plug can be changed from the primary faceplate side for mixture ratio adjustments and maintenance. The lox post is an integral part from the weld at the lox dome to the tip at the primary faceplate to avoid leakage into the hot gas side. The lox plug produces an annular lox jet inside the much faster hot gas jet.

The primary and secondary faceplates are held together by the hot gas shroud assembly (Fig. 7). The shroud directs and shapes the gas flow into an annular jet around the annular lox jet. The shroud is mounted to the lox post and can be changed from the primary faceplate side for mixture ratio adjustments and maintenance.

The diameter for closest element spacing is 2 in. for the low loss injector (Fig. 7) and 0.63 in. for the present design (Fig. 4). The lox post outer and inner diameters are 1.25 and 0.80 in. in the proposed and 0.329 and 0.188 in. in the present design. The lox sieve of the lox plug has 36 holes with a 0.084 in. diameter. The hot gas sieve in the shroud has 48 slanted and well rounded holes of 0.20 in. diameter. The lox post lengths between the lox dome and the secondary faceplate are 5.935 in. at the injector perifery and 3.334 in. at the injector center in both designs.

The lox post is assumed clamped at the weld and hinged at the secondary faceplate to conservatively assess bending stresses. The large element diameters admit larger corner radii to reduce stress concentrations. Also bending stresses due to hot gas flow are tenfold reduced, e.g., the maximum stress due to drag is now 3800 psi. The lox post first bending mode frequency is 5474 Hz versus a vortex frequency of 2321 Hz according to a Strouhal number of 0.31. The fundamental vortex frequency is below and well detuned, which is not the case in the present design where the first bending mode is 1200 Hz while the vortex frequency according to Strouhal is at 6164 Hz among the higher modes. The proposed design also reduces the axial and the hoop stresses to 1452 and 804 psi, which is approximately half of the present design values.

DESIGN CONSIDERATIONS

The coaxial injection approach was followed here because of its stable combustion effect. The intersection of oxidizer and fuel jets is well distributed and less sensitive to pressure, e.g., the focus of impinging jets. The velocities of the fuel is considerably (20 times) larger than the oxidizer jet for effective mixing. Additionally, the low loss elements have extremely rough surfaces on both sides of the lox post tips (Fig. 7) which separate the propellants. The roughness induces turbulent layers between the emerging jets of the oxidizer and the fuel. Mixing is enhanced and contained by the impulse of the much swifter moving layers of both propellants.

Turbulent flow due to Reynolds numbers of 10^6 makes the pressure loss proportional to dynamic pressure or velocity square as in the present design. The quadratic relationship reduces the pressure sensitivity of velocity changes two times.

Individual flow control devices for each element could help stability, but this option was abandoned because of the unavoidable inertial coupling with vibrations. Also abandoned was the design of most densely stacked elements requiring diameters that grow from row to row in a geometrical sequence. Instead, large diameter elements of equal size, stacked in a circularized hexagonal pattern (Fig. 8) were selected.

Large diameter elements solve the stress problem, uncouple the vortex frequencies, and damp acoustic resonances. However, large diameters reduce the mixing contour length M as the equations (1) through (5) show.

$$M = N \pi L \tag{1}$$

$$N = 3R\,(R+1) \tag{2}$$

$$C = D\,(2R+1) \quad , \quad R = (C/D - 1)/2 \tag{3}$$

$$N = 0.75\,[(C/D)^2 - 1] \tag{4}$$

$$M = 0.75\,\pi\,C\,(C/D - D/C)\,L/D \tag{5}$$

where

C = chamber inner diameter (17.74 in.)

D = element closest spacing diameter (2 versus 0.63 in.)

L = lox post tip inner diameter (0.8 versus 0.188 in.)

M = propellant mixing contour length (151 versus 354 in.)

R = circle row number (4 versus 13)

The parenthesis are the proposed versus the present design values. The new M of 151 in. is a factor 2.34 less than the present M of 354 in. However, recirculation within the annular lox jet reduces the factor to approximately 1.17 which makes the proposed elements equivalent to 10 elements of the present design. In other words, the new element is a continuous version of the 10 smaller diameter elements. The M can be doubled by a 60 degree corrugation in the contour, e.g., by machining axial grooves into the outer surface of the lox plug and the inner surface of the fuel shroud (not shown in Fig. 7).

INJECTION STABILITY

Stability is of major concern because low loss injectors operate with lower than usual injection pressure losses. The pressure loss is directly related to the feedback gain as equations (6) through (36) explain.

$$p_C = g_L \dot{w}_L + g_H \dot{w}_H = g_L \rho_L A_L v_L + g_H \rho_H A_H v_H \tag{6}$$

$$f_L \rho_L u_L^2/2 = p_L - p_C - \dot{v}_L m_L \tag{7}$$

$$f_H \rho_H u_H^2/2 = p_H - p_C - \dot{v}_H m_H \tag{8}$$

$$dp_C = g_L \rho_L A_L dv_L + g_H \rho_H A_H dv_H \tag{9}$$

$$du_L = (dp_L - dp_C - dv_L s m_L)/f_L \rho_L u_L \tag{10}$$

$$du_H = (dp_H - dp_C - dv_H s m_H)/f_H \rho_H u_H \tag{11}$$

$$dp_C = (du_L - dv_L) k_L/s - dv_L s m_L \tag{12}$$

$$dp_C = (du_H - dv_H) k_H/s - dv_H s m_H \tag{13}$$

$$k_L = \omega_L^2 m_L \tag{14}$$

$$k_H = \omega_H^2 m_H \tag{15}$$

$$\omega_L = 2 \pi c_L/4b_L = \pi c_L/2b_L \tag{16}$$

$$\omega_H = 2 \pi c_H/4b_H = \pi c_H/2b_H \tag{17}$$

$$m_L = \rho_L b_L/2 \tag{18}$$

$$m_H = \rho_H b_H/2 \tag{19}$$

$$dv_L = (du_L - dp_C\, s/k_L) / (1 + s^2/\omega_L{}^2) \tag{20}$$

$$dv_H = (du_H - dp_C\, s/k_H) / (1 + s^2/\omega_H{}^2) \tag{21}$$

$$dv_L = [(dp_L - dp_C\,(1 + s\,\tau_L)] / [f_L\,\rho_L\,u_L\,(1 + s\,\tau_L{}' + s^2/\omega_L{}^2)] \tag{22}$$

$$dv_H = [(dp_H - dp_C\,(1 + s\,\tau_H)] / [f_H\,\rho_H\,u_H\,(1 + s\,\tau_H{}' + s^2/\omega_H{}^2)] \tag{23}$$

$$\tau_L = f_L\,\rho_L\,u_L/k_L = 8\,f_L\,u_L\,b_L/(\pi\,c_L)^2 \tag{24}$$

$$\tau_H = f_H\,\rho_H\,u_H/k_H = 8\,f_H\,u_H\,b_H/(\pi\,c_L)^2 \tag{25}$$

$$\tau_L{}' = m_L/f_L\,\rho_L\,u_L = b_L/(2f_L\,u_L) \tag{26}$$

$$\tau_H{}' = m_H/f_H\,\rho_H\,u_H = b_H/(2f_H\,u_H) \tag{27}$$

$$dp_C = G_L\,[dp_L - dp_C\,(1 + s\,\tau_L)] / (1 + s\,\tau_L{}' + s^2/\omega_L{}^2)$$

$$+ G_H\,[dp_H - dp_C\,(1 + s\,\tau_H)] / (1 + s\,\tau_H{}' + s^2/\omega_H{}^2) \tag{28}$$

$$G_L = g_L\,\rho_L\,A_L/f_L\,\rho_L\,u_L = g_L\,\dot{w}_L/2\Delta p_L \tag{29}$$

$$G_H = g_H\,\rho_H\,A_H/f_H\,\rho_H\,u_H = g_H\,\dot{w}_H/2\Delta p_H \tag{30}$$

$$dp_C\,[1 + G_L(1 + s\,\tau_L) / (1 + s\tau_L{}' + s^2/\omega_L{}^2) + G_H\,(1 + s\,\tau_H) / (1 + s\,\tau_H{}' + s^2/\omega_H{}^2)]$$

$$= dp_L\,G_L/(1 + s\,\tau_L{}' + s^2/\omega_L{}^2) + dp_H\,G_H/(1 + s\,\tau_H{}' + s^2/\omega_H{}^2) \tag{31}$$

$$G = 1 + G_L + G_H + s\,[G_L\,\tau_L + G_H\,\tau_H + (1 + G_L)\tau_H{}' + (1 + G_H)\,\tau_L{}'] + s^2\,(G_L\,\tau_L\,\tau_H{}'$$

$$+ G_H\,\tau_H\,\tau_L{}' + \tau_L{}'\,\tau_H{}' + (1 + G_L)/\omega_H{}^2 + (1 + G_H)/\omega_L{}^2] + s^3\,(G_L\,\tau_L/\omega_H{}^2$$

$$+ G_H\,\tau_H/\omega_L{}^2 + \tau_L{}'/\omega_H{}^2 + \tau_H{}'/\omega_L{}^2) + s^4/(\omega_L\,\omega_H)^2 \tag{32}$$

$$E_L = G_L/(1 + G_L + G_H) \tag{33}$$

$$E_H = G_H/(1 + G_L + G_H) \tag{34}$$

$$E = 1 + s[E_L \tau_L + E_H \tau_H + (1 - E_L) \tau_L' + (1 - E_H) \tau_H'] + s^2 [E_L \tau_L \tau_H' + E_H \ H \tau_L' + (1 - E_L - E_H) \tau_L' \tau_H' + (1 - E_L)/\omega_L^2 + (1 - E_H)/\omega_H^2] + s^3 [E_L \tau_L/\omega_H^2 + E_H \tau_H/\omega_L^2 + (1 - E_L - E_H) (\tau_L'/\omega_H^2 + \tau_H'/\omega_L^2)] + s^4 (1 - E_L - E_H)/(\omega_L \omega_H)^2 \tag{35}$$

$$dp_C = dp_L E_L (1 + s \tau_H' + s^2/\omega_H^2) / E + dp_H E_H (1 + s \tau_L' + s^2/\omega_L^2) / E \tag{36}$$

where

A_L, A_H = injection areas

b_L, b_H = injection cavity depths

c_L, c_H = sound velocities

E = normalized characteristic equation

E_L, E_H = closed loop pressure gains

f_L, f_H = injection loss factors

G = characteristic equations

g_L, g_H = mass flow gains

G_L, G_H = open loop pressure gains

H = index for hot gas

k_L, k_H = generalized injection flow stiffnesses

L = index for lox

m_L, m_H = generalized injection flow masses

p_C = combustion chamber pressure

p_L, p_H = manifold pressures

u_L, u_H = equivalent friction velocities

v_L, v_H = injection velocities

$\dot{w}_L$, $\dot{w}_H$ = injected mass flows

Δp_L, Δp_H = injection pressure losses

ρ_L, ρ_H = mass densities

τ_L, τ_H = injection time constants

τ_L', τ_H' = damping time constants

ω_L, ω_H = injection cavity resonances in radians

Equation (6) relates the lox and the hot gas mass flows in a linearized form to the MCC chamber pressure. Equations (7) and (8) are the injection friction losses for lox (index L) and hot gas (index H). Equations (9) through (13) are differentials to express small variations in Laplace transform. Equation (9) is the differential of equation (6). Equations (10) and (11) follow from the differentials of equations (7) and (8). Equations (12) and (13) are the Laplace transform of the differential responses from the 1/4 wave length injection cavities. Only the first mode is considered. Equations (14) and (15) are the generalized fluid stiffnesses. Equations (16) and (17) are the 1/4 wave length resonance frequencies. Equations (18) and (19) are the generalized fluid masses of the injection cavities. Equations (20) and (21) result from equations (12) and (13) after rearranging and substituting with equations (14) through (19). Equations (22) and (23) follow from equations (20) and (21) after substituting with equations (10) and (11). The resulting time constants are found in equations (24) through (27). Equation (28) is obtained from equation (9) after substituting with equations (22) and (23). Equations (29) and (30) define the open loop pressure gains and show the relationship to the injection pressure losses. Equation (31) follows from rearranging equation (28). Equation (32) is the characteristic equation for the explicit chamber pressure. Equations (33) and (34) are the closed loop pressure gains for lox and hot gas. Equation (35) follows from equation (32) after dividing by $1+G_L + G_H$ and substituting with equations (33) and (34). Equation (36) follows from rearranging equation (31) and substituting with equations (33) through (35).

The gains E_L and E_H are always less than one due to the negative feedback of p in equation (28), i.e., p resists the injection flow. G_L and G_H are larger than one and are inversely proportional to the injection pressure losses as equations (29) and (30) show. In other words the gains become lower as the pressure losses are increased. Thus, the pressure losses become an important design criterion. Furthermore, the gains increase when throttling because the pressure drop is proportional to velocity power with an exponent between 1 and 2, while mass flow is proportional to velocity. Equation (36) helps to assess the injection stability versus gain according to the roots of equation (35).

Table 1 shows SSME gains for the present versus the proposed designs. The proposed design considerably increases the open loop gains G_L and G_H while the closed loop gains E_L and E_H are only 5 percent and 20 percent higher. The changes are negligible for the pogo loop, i.e., thrust to propellant acceleration feedback loop. Table 2 gives injection stability roots for the present and the proposed designs. The proposed design is most stable as the b_L = 2.4 in. cases indicate by the highest damping factors (zeta).

The f_1 and f_2 roots indicate that the proposed design responds considerably faster because of less lag. Both designs are about aperiodic for the rather simple model. More details are needed to fully analyze stability. Combustion is not instant as expressed by the constant mass flow gains g_L and g_H in equation (6). The acoustic response of the combustion chamber cannot be neglected but must be included to prove that low loss injector elements add sufficient damping. The removal of the baffles drops the first transverse mode to about 2000 Hz which is within the damping range of the injector elements.

ADVANTAGES

Low loss injector elements increase SSME thrust and space shuttle payload. The selected large element diameter reduces bending stresses tenfold which increases service life. Manufacturing cost should be less due to relaxed tolerances and a tenfold reduction on elements. Maintenance and development is helped since the flow metering components are exchangeable from the primary faceplate side. The injector modification should fit within the same forging of the SSME powerhead.

Baffles and acoustic absorbers can be eliminated due to the damping provided by the large diameter injector elements which cover 38 percent of the combustion chamber's surface and thus are more effective than a narrow band of absorbers. Low loss injector elements are coaxial and thus should benefit from past experience.

FUTURE PLANS

A patent application was filed in October 1983. The analysis of acoustic damping will be next, with combustion and mixing models following. Simultaneously, analysis, fabrication of three elements, and small scale testing should be contracted as soon as funds can be made available. The complexity warrants some duplication between contractors and the government to penetrate difficult areas.

CONCLUSION

The feasibility of low loss injectors is explored. Stability with lower injection losses seems feasible by designing the elements as effective dampers. Large diameter injector elements promise longevity and less cost. Ways of improved mixing are identified. Further development is recommended, especially when retrofitting appears feasible and payload can be gained.

TABLE 1. FULL POWER LEVEL SSME GAINS

Design	g_L $\frac{1}{in.s}$	g_H $\frac{1}{in.s}$	$\dot{w}_L$ $\frac{lb.s}{in.}$	$\dot{w}_H$ $\frac{lb.s}{in.}$	Δp_L psi	Δp_H psi	G_L /	G_H /	E_L /	E_H /
Present	888	1745	2.211	0.636	694	334	1.415	1.662	0.347	0.408
Proposed	888	1745	2.166	0.734	400	200	2.404	3.203	0.364	0.485

TABLE 2. FULL POWER LEVEL SSME STABILITY

Design	Present		Proposed					
b_L in.	6.41	9.01	2.40	6.41	9.01	2.40	6.41	9.01
b_H in.	2.75	2.75	2.75	2.75	2.75	4.10	4.10	4.10
f_1 Hz	892	645	3087	1348	997	2903	1275	951
f_2 Hz	3034	2149	5635	2036	1415	4886	2093	1455
f_3 Hz	4870	4865	5034	5610	5717	3418	3635	3746
$zeta_3$	0.87	0.87	0.93	0.90	0.89	0.94	0.91	0.90

b_L is the lox injection cavity length from orifice to tip.

b_H is the hot gas injection cavity length of the shroud.

f_1, f_2 are the -3 db corner frequencies of 1st order roots.

f_3 is a nearly aperiodic root frequency with damping zeta.

$zeta_3$ is the damping factor (critical damping zeta = 1).

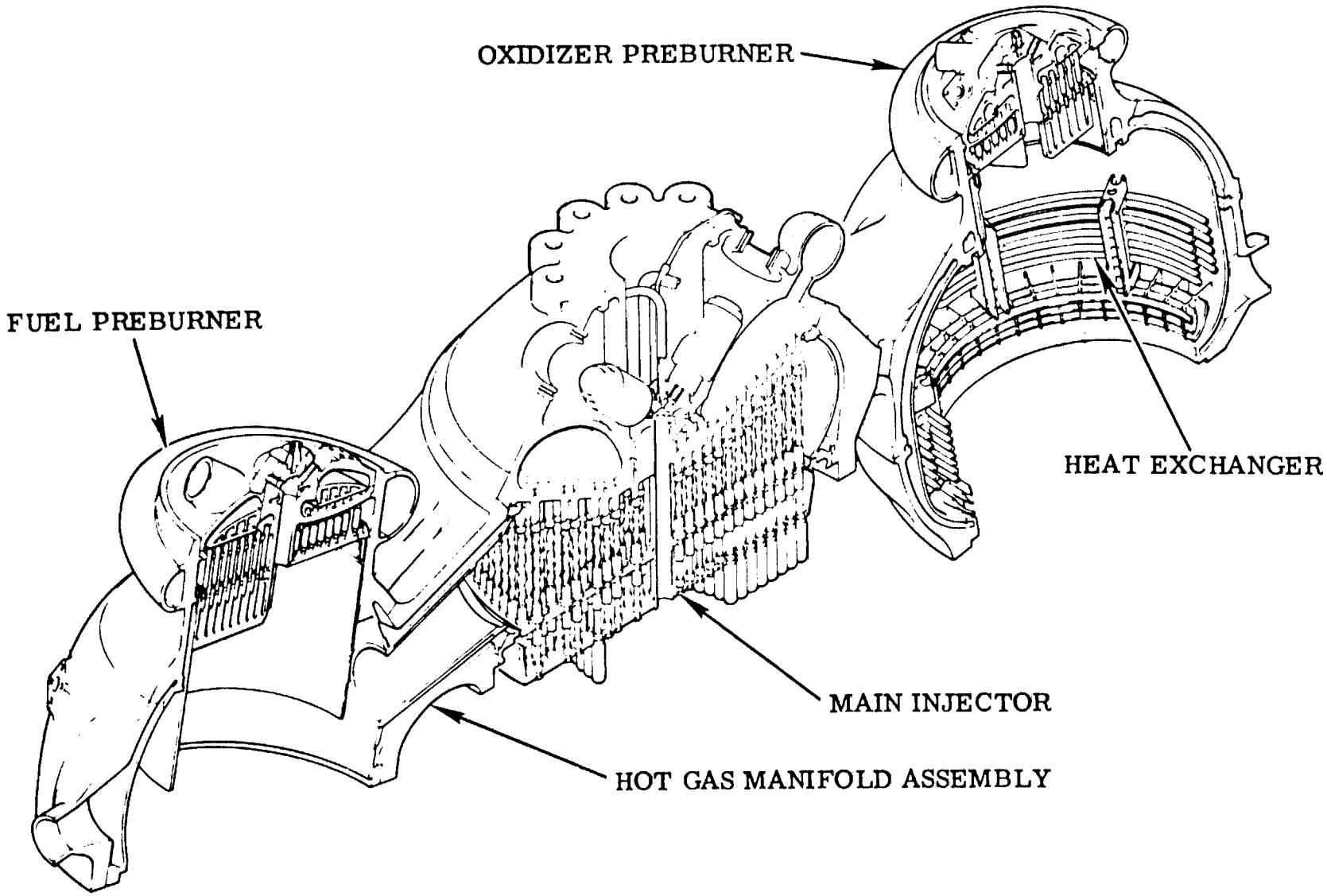

Figure 1. Powerhead assembly.

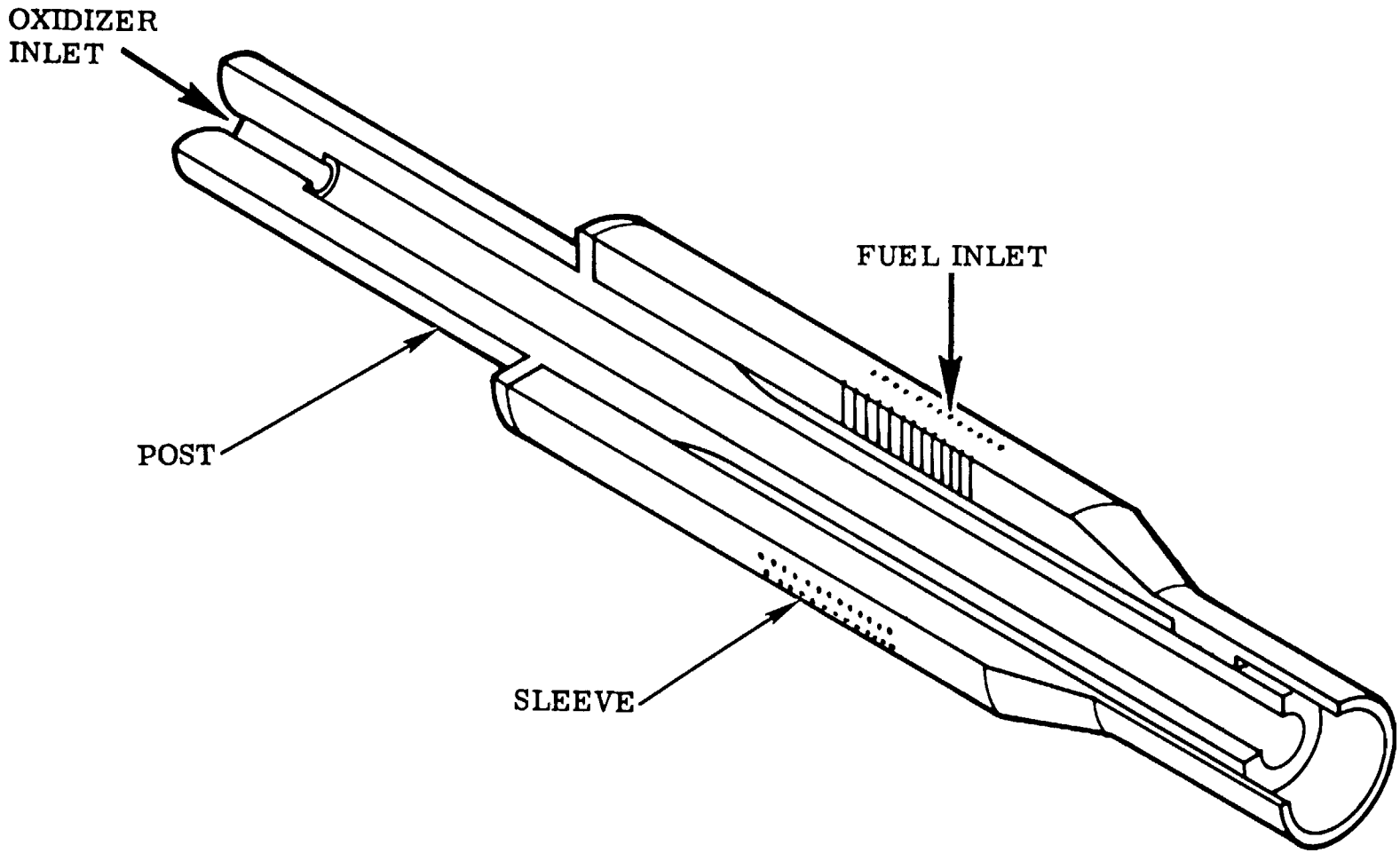

Figure 2. Preburner injector element.

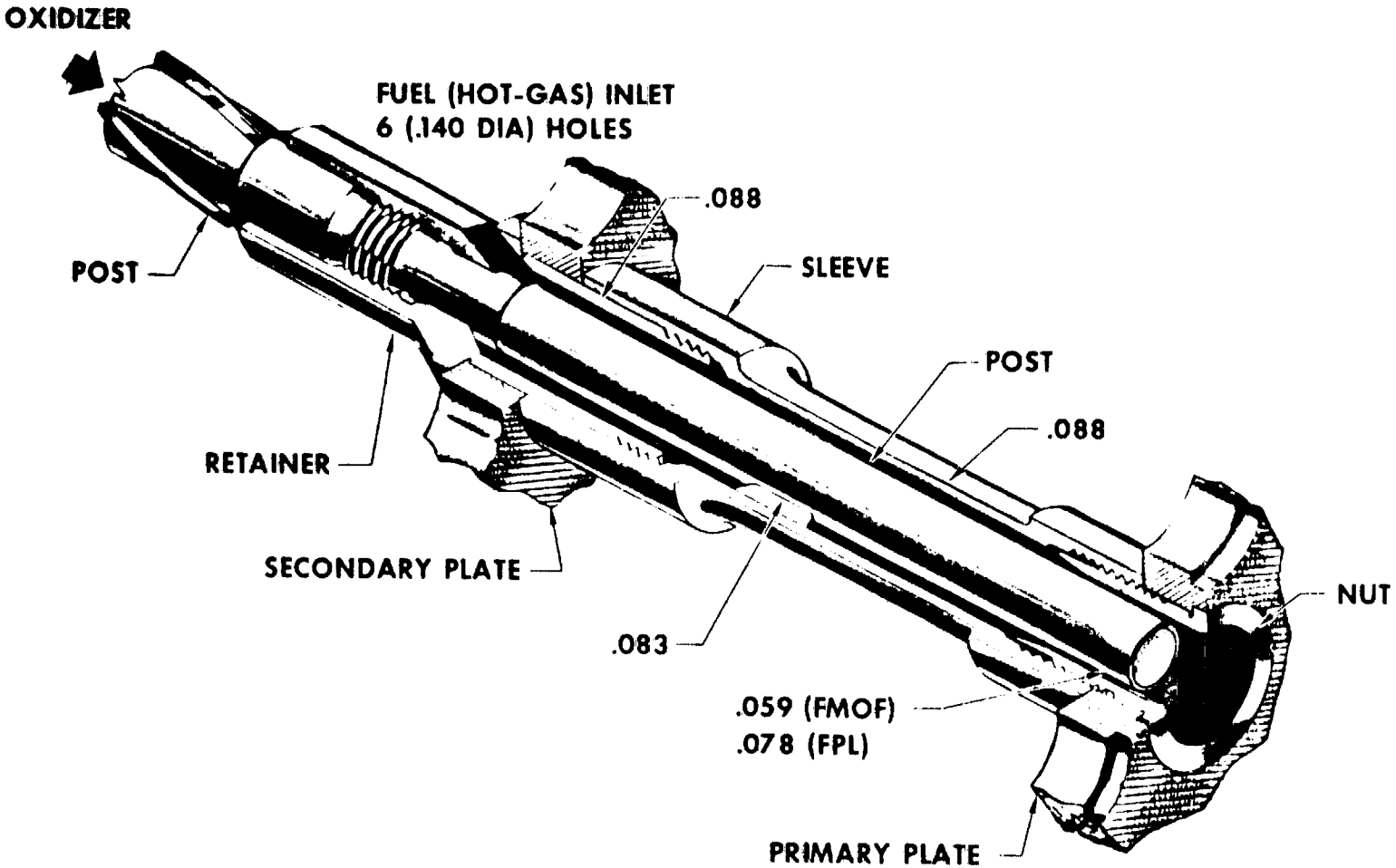

Figure 3. Main injector element.

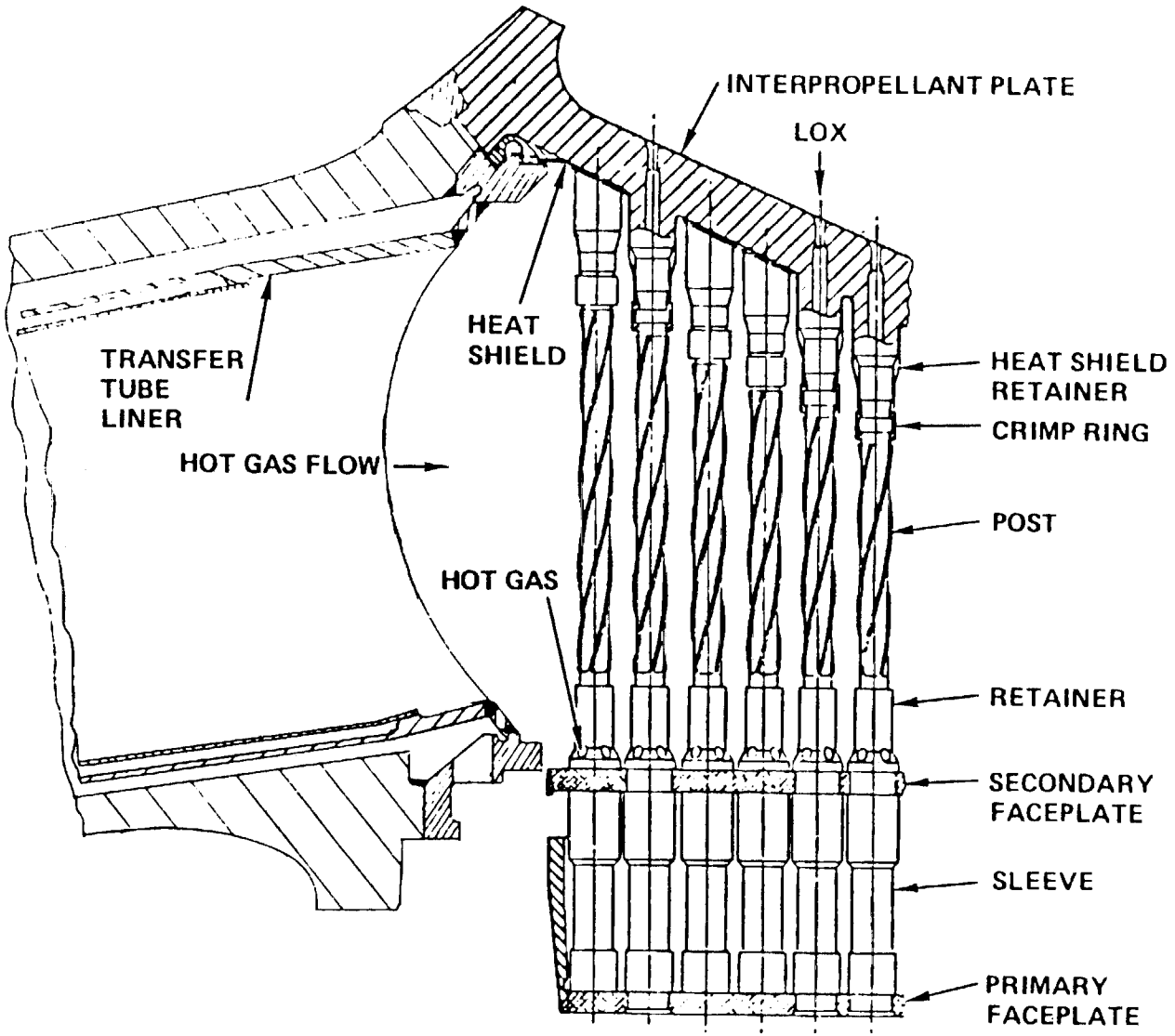

Figure 4. Hardware description.

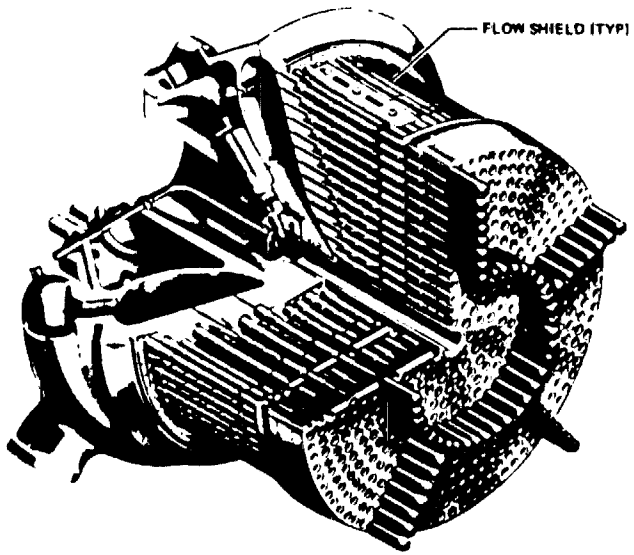

GEOMETRY

■ 347 CRES RIGIMESH FACEPLATES	
■ DUAL SPARK IGNITER	
■ FACE DIAMETER	17.74 IN.
■ INJECTOR CONFIGURATION	CONCENTRIC ORIFICE
■ NUMBER OF ELEMENTS	525
■ NUMBER OF FLOW SHIELDS	42
■ NUMBER OF BAFFLE ELEMENTS	75
■ BAFFLE ELEMENT LENGTH	2 IN.

OPERATING PARAMETERS (FPL, MR-6.0)

■ CHAMBER PRESSURE	3277 PSIA
■ OXIDIZER FLOWRATE	854.6 LB/SEC
■ HOT GAS FLOWRATE	249.4 LB/SEC
■ COOLANT FLOWRATE	
■ PRIMARY FACEPLATE	5.2 LB/SEC
■ SECONDARY FACEPLATE	3.2 LB/SEC
■ BAFFLES	15.1 LB/SEC
■ FILM COOLANT	3.8 LB/SEC
■ ACOUSTIC CAVITY	1.4 LB/SEC

Figure 5. Main injector.

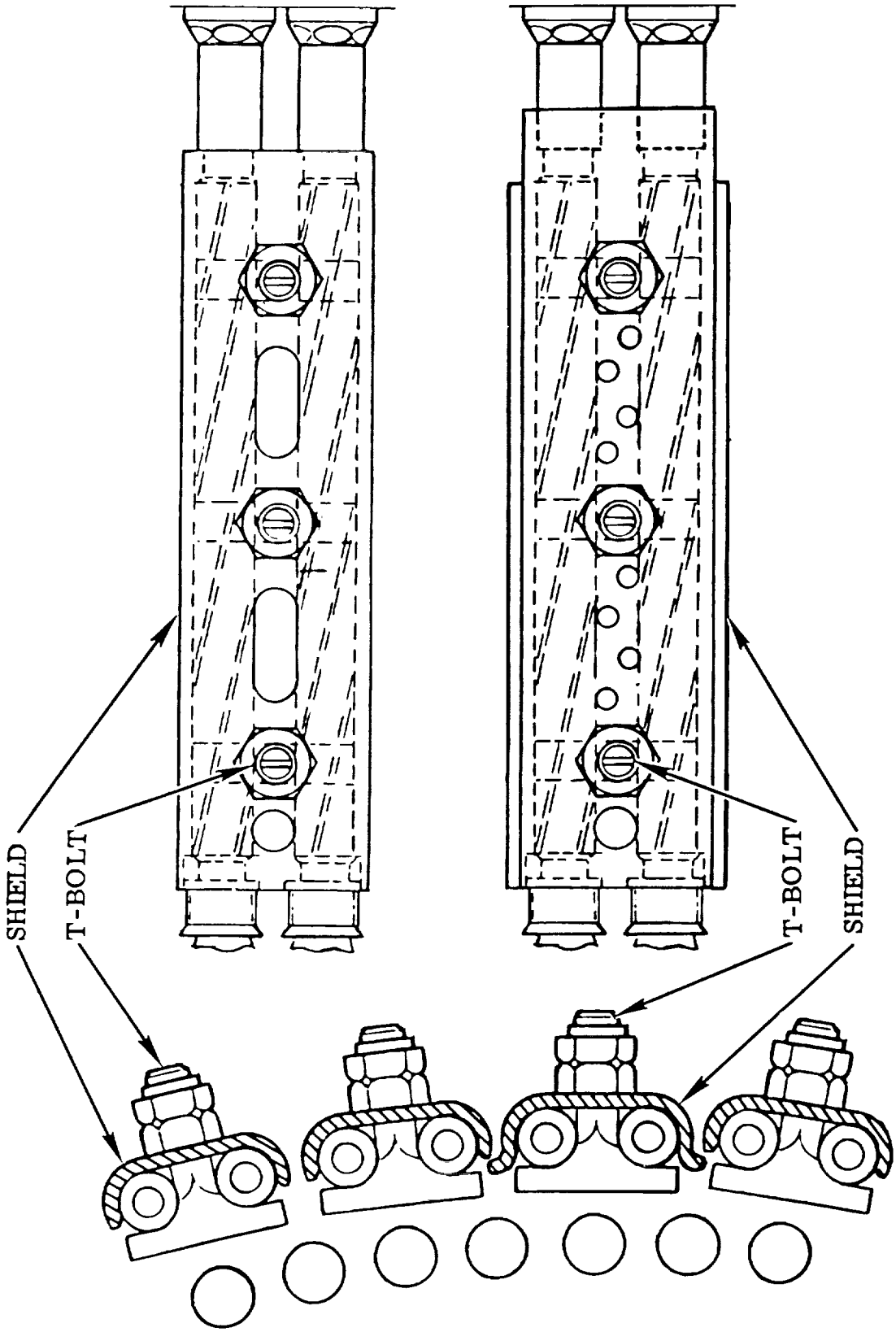

Figure 6. Main injector lox post flow shield.

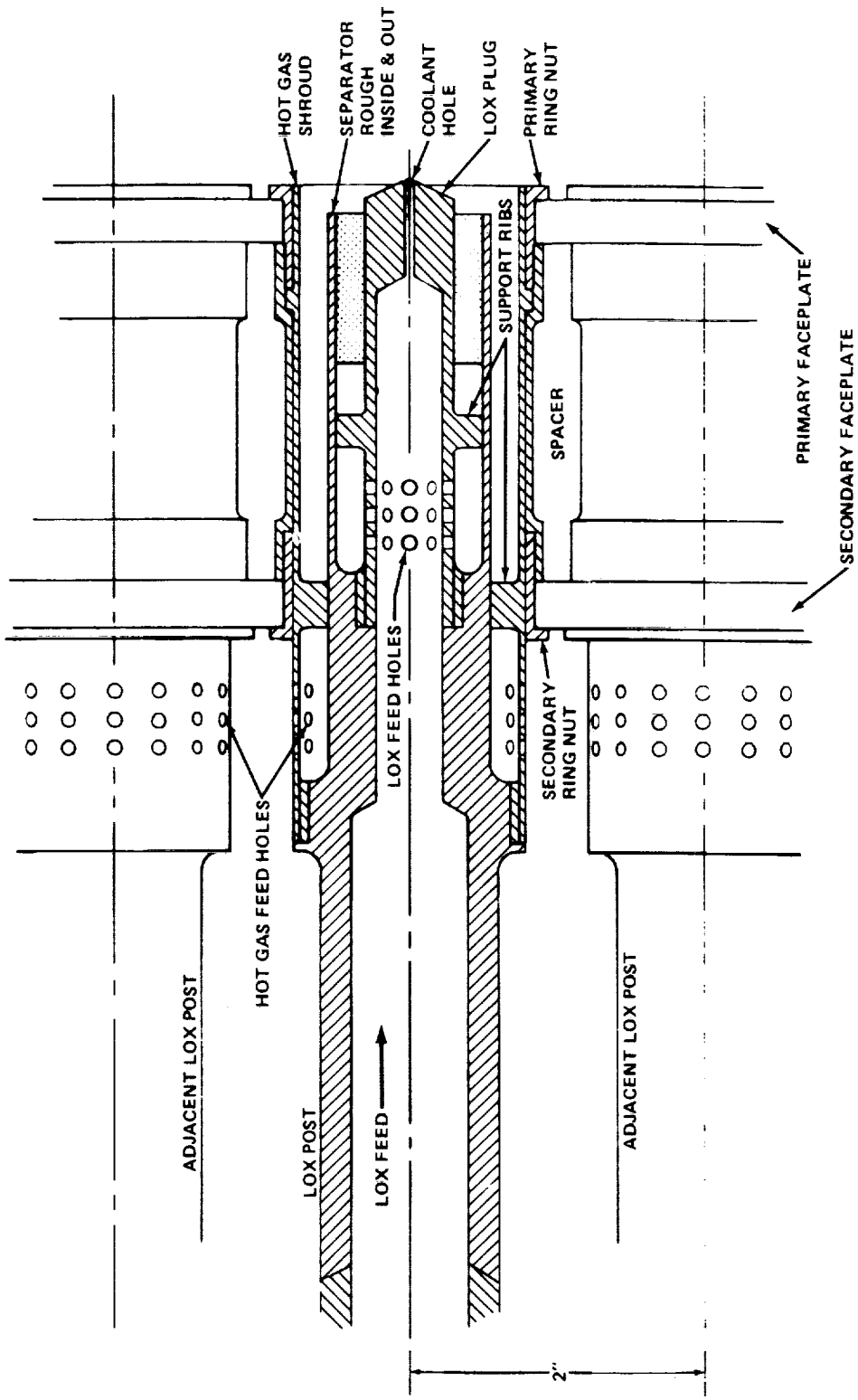

Figure 7. Low loss injector element for main combustion chamber.

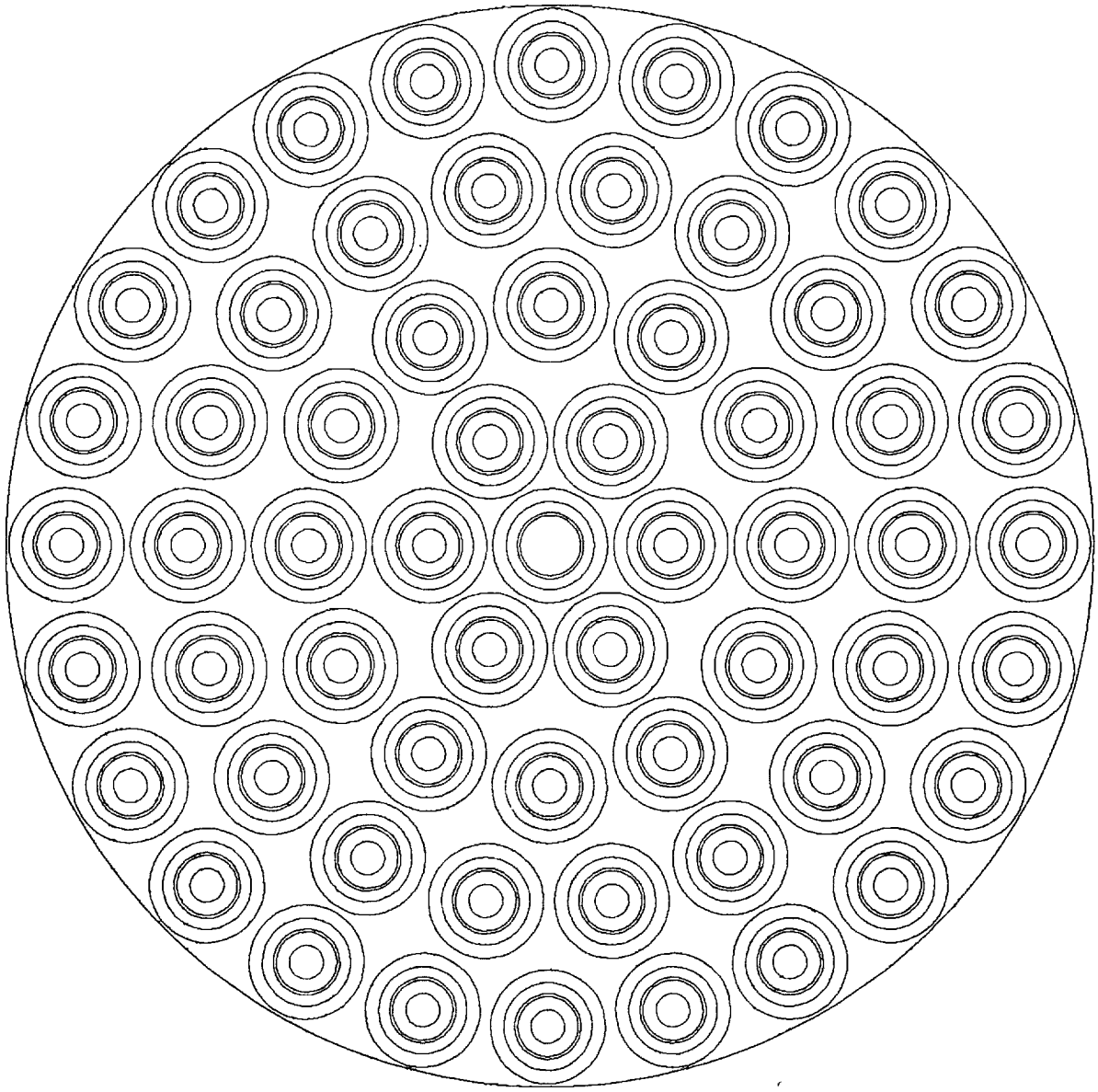

Figure 8. Circularized hexagonal pattern of main low loss injector.

APPROVAL

LOW LOSS INJECTOR FOR SPACE SHUTTLE MAIN ENGINE

By George L. von Pragenau

The information in this report has been reviewed for technical content. Review of any information concerning Department of Defense or nuclear energy activities or programs has been made by the MSFC Security Classification Officer. This report, in its entirety, has been determined to be unclassified.

GEORGE F. McDONOUGH
Director, Systems Dynamics Laboratory

☆ U.S. GOVERNMENT PRINTING OFFICE 1984—746-070/155